Three-Dimensional Object Matching in Mobile Laser Scanning Point Clouds

Article *in* IEEE Geoscience and Remote Sensing Letters · February 2015

DOI: 10.1109/LGRS.2014.2347347

Yongtao Yu
Huaiyin Institute of Technology
41 PUBLICATIONS **370** CITATIONS

Jonathan Li
University of Waterloo
252 PUBLICATIONS **3,240** CITATIONS

Haiyan Guan
Nanjing University of Information Science & …
52 PUBLICATIONS **428** CITATIONS

Cheng Wang
Xiamen University
157 PUBLICATIONS **894** CITATIONS

Three-Dimensional Object Matching in Mobile Laser Scanning Point Clouds

Yongtao Yu, Jonathan Li, *Senior Member, IEEE*, Haiyan Guan, Fukai Jia, and Cheng Wang, *Member, IEEE*

***Abstract*—This letter presents a 3-D object matching framework to support information extraction directly from 3-D point clouds. The problem of 3-D object matching is to match a template, represented by a group of 3-D points, to a point cloud scene containing an instance of that object. A locally affine-invariant geometric constraint is proposed to effectively handle affine transformations, occlusions, incompleteness, and scales in 3-D point clouds. The 3-D object matching framework is integrated into 3-D correspondence computation, 3-D object detection, and point cloud object classification in mobile laser scanning (MLS) point clouds. Experimental results obtained using the 3-D point clouds acquired by a RIEGL VMX-450 system showed that completeness, correctness, and quality of over 0.96, 0.94, and 0.91 are achieved, respectively, with the proposed framework in 3-D object detection. Comparative studies demonstrate that the proposed method outperforms the two existing methods for detecting 3-D objects directly from large-volume MLS point clouds.**

***Index Terms*—Mobile laser scanning (MLS), object classification, point cloud, 3-D object detection, 3-D object matching.**

I. Introduction

THE acquisition and processing of huge volumes of highly dense and irregularly distributed 3-D point clouds from mobile laser scanning (MLS) systems has received increasing attention over the past few years [1]. Automated detection and extraction of objects from such 3-D point clouds has been a very active research topic in the remote sensing community [2]–[6]. A pairwise 3-D shape context was developed in [2], for modeling geometric features of point cloud objects. Such shape context was successfully applied to extract 3-D light poles and trees from MLS point clouds. Hough forest was proposed in [3] to learn mappings from patch features to object centroids. This method obtained promising results in detecting 3-D light poles, palm trees, cars, and traffic signposts from MLS point clouds. A principal component analysis (PCA)-based approach was introduced in [7], for distinguishing trees and buildings. The identified buildings were further processed to extract building footprints based on an integration of random sample consensus (RANSAC) and PCA. In [8], man-made objects were identified from MLS point clouds using a layer-wise approach that sliced the raw point clouds into three layers and classified seed points into different man-made object categories within each layer. Recently, some other studies have been conducted for the detection and extraction of windows [9], railway tracks [10], roads [11], and vertical walls [12] from MLS point clouds.

Rather than handling highly dense 3-D point clouds, some researchers rasterized the 3-D MLS point clouds into 2-D georeferenced feature images. Therefore, existing image processing methods were adopted to achieve the detection of various objects. In [13], road surface point clouds were first converted into georeferenced intensity images through inverse distance weighted interpolation. Then, road markings were extracted using multithresholding and refined through morphological operations. A marked point process of rectangles and disks was developed in [4], for detecting road manholes and sewer well covers from georeferenced intensity images.

In this letter, we develop a framework for matching 3-D objects in 3-D MLS point clouds, directly. A locally affine-invariant geometric constraint is proposed to improve the performance of point-set-based 3-D object matching. The 3-D object matching framework is embedded into the applications of 3-D correspondence computation, 3-D object detection, and point cloud object classification from 3-D point clouds acquired by a RIEGL VMX-450 system.

II. 3-D Object Matching Framework

A. Problem Formulation

The problem of object matching from point clouds is defined as matching a group of template feature points that represent an object to a group of scene feature points that represent a scene containing an instance of that object. Here, a feature point is a 3-D point sampled from either the template or the scene. First, a group of feature points is selected from the template and scene point clouds, respectively. Denote n_T and n_S $(n_\mathrm{T} \leq n_\mathrm{S})$ as the number of template and scene feature points, respectively. Let $\mathbf{T} \in R^{n_\mathrm{T} \times 3}$ and $\mathbf{S} \in R^{n_\mathrm{S} \times 3}$ be the matrices recording the 3-D coordinates of the template and scene feature points, respectively. The goal of object matching is to determine a matching function $f(\cdot)$ that 1) matches each template feature point $p_i = (x_i, y_i, z_i) \in R^3, i = 1, \ldots, n_\mathrm{T}$ to a scene feature point $q_j = (x_j, y_j, z_j) \in R^3, j = 1, \ldots, n_\mathrm{S}$ and 2) minimizes the following overall objective function containing both feature and geometric matching costs:

$$\min_{f} \sum_{i=1}^{n_\mathrm{T}} \left\{ c\left(p_i, f(p_i)\right) + \lambda \cdot g\left(p_i, N_{p_i}; f(p_i), N_{f(p_i)}\right) \right\} \quad (1)$$

where $c(p, q)$ denotes the feature matching cost between point p and point q; N_{p_i} is the local neighborhood of point p_i; $g(\cdot)$

Manuscript received May 3, 2014; revised June 16, 2014 and July 18, 2014; accepted August 9, 2014. This work was supported by the National Natural Science Foundation of China under Grant 41471379. *(Corresponding author: Jonathan Li.)*

Y. Yu, F. Jia, and C. Wang are with the Fujian Key Lab of Sensing and Computing for Smart Cities, Xiamen University, Xiamen FJ 361005, China.

J. Li is with the MoE Key Laboratory of Underwater Acoustic Communication and Marine Information Technology, Xiamen University, Xiamen FJ 361005, China (e-mail: junli@xmu.edu.cn).

H. Guan is with the Department of Geography and Environmental Management, University of Waterloo, Waterloo, ON N2L 3G1 Canada.

Color versions of one or more of the figures in this paper are available online at http://ieeexplore.ieee.org.

Digital Object Identifier 10.1109/LGRS.2014.2347347

represents a geometric matching cost function that measures the dissimilarity between two sets of ordered points $\{p_i, N_{p_i}\}$ and $\{f(p_i), N_{f(p_i)}\}$; λ controls the relative weight between the feature and geometric matching costs.

B. Feature Matching Cost

The persistent feature histogram (PFH) [14] has proved to be a robust and highly distinctive feature descriptor for discrete point clouds. A PFH is based on the relationships between the points in the k-neighborhood and their estimated surface normals. By generalizing the mean curvature around a point, a multidimensional histogram is constructed to model the interactions between the directions of the estimated normals. The PFH descriptor results in a 16-D histogram descriptor for each feature point. Denote $h_p \in R^{16}$ as the PFH descriptor for feature point p. Then, the cost of matching a template feature point p to a scene feature point q is defined using χ^2 distance [15] as follows:

$$c(p,q) = \sum_{k=1}^{16} \frac{[h_p(k) - h_q(k)]^2}{h_p(k) + h_q(k)}. \tag{2}$$

The feature matching costs are stored in a feature matching cost matrix $\mathbf{C} \in R^{n_\mathrm{T} \times n_\mathrm{S}}$, whose entry $C_{ij} = c(p_i, q_j), i = 1, 2, \ldots, n_\mathrm{T}, j = 1, 2, \ldots, n_\mathrm{S}$ stores the cost of matching the ith template feature point to the jth scene feature point.

The matching function $f(\cdot)$ is usually modeled as a binary variable matrix $\mathbf{X} \in \{0,1\}^{n_\mathrm{T} \times n_\mathrm{S}}$, as follows:

$$f(p_i) = q_j \Leftrightarrow X_{ij} = 1,\ i = 1, 2, \ldots, n_\mathrm{T},\ j = 1, 2, \ldots, n_\mathrm{S}. \tag{3}$$

$X_{ij} = 1$ (or zero) indicates that the ith template feature point is matched (or not matched) to the jth scene feature point. Because each template feature point is matched to exactly one scene feature point, each row of $\mathbf{X}$ contains exactly one entry with a value of 1.

By integrating the feature matching cost matrix $\mathbf{C}$ and the binary variable matrix $\mathbf{X}$, the feature matching cost term in (1) is expressed as

$$\sum_{i=1}^{n_\mathrm{T}} c\left(p_i, f(p_i)\right) = \mathrm{tr}(\mathbf{C}\mathbf{X}^T) = \sum_{i=1}^{n_\mathrm{T}} \sum_{j=1}^{n_\mathrm{S}} C_{ij} X_{ij}. \tag{4}$$

For the ith row of $\mathbf{X}$, the column index of the entry with a value of 1 specifies the index of the scene feature point matched to the template feature point p_i. Let $\mathbf{X}_i$ denote the ith row of $\mathbf{X}$. Then, $\mathbf{X}_i\mathbf{S}$ computes the coordinates of the matched scene feature point for p_i. Combining all rows of $\mathbf{X}$, $\mathbf{XS}$ represents the coordinates of all matched scene feature points in the same order as the template feature points.

C. Locally Affine-Invariant Geometric Constraint

Considering the affine transformations, occlusions, incompleteness, and scales, the geometric matching cost function $g(\cdot)$ in (1) is modeled by locally affine-invariant geometric constraints. We assume that each template feature point p_i can be exactly represented by an affine combination of its neighbors as follows:

$$p_i = \sum_{p_j \in N_{p_i}} W_{ij} p_j \tag{5}$$

where N_{p_i} is the local neighborhood of point p_i; $\mathbf{W}$ is a $n_\mathrm{T} \times n_\mathrm{T}$ weight matrix that records the affine combination coefficients for all template feature points. Denote $\mathbf{W}_i$ as the ith row of $\mathbf{W}$. Then, $\mathbf{W}_i$ depicts the local geometric layout round p_i. The following constraints are placed on $\mathbf{W}$: 1) $W_{ij} = 0$ if $p_j \notin N_{p_i}$, and 2) each row must add up to one. The first constraint reflects a point's local geometric property; the second constraint makes the representation invariant to global transformations. These two constraints guarantee that a feature point is always exactly represented by the affine combination of its neighbors [16]. By using the locally affine-invariant geometric constraints, the geometric matching cost term in (1) is defined as

$$\sum_{i=1}^{n_\mathrm{T}} g\left(p_i, N_{p_i}; f(p_i), N_{f(p_i)}\right) = \|(\mathbf{I} - \mathbf{W})\mathbf{XS}\|_1 \tag{6}$$

where $\|\cdot\|_1$ denotes the summation of absolute values of all the entries in a matrix.

D. Overall Objective Function

By combining the feature and geometric matching costs in (4) and (6), we define the overall objective function for point cloud object matching as follows:

$$\begin{aligned} &\underset{\mathbf{X}}{\text{minimize}}\ \mathrm{tr}(\mathbf{C}\mathbf{X}^T) + \lambda \|(\mathbf{I} - \mathbf{W})\mathbf{XS}\|_1 \\ &\text{subject to}\ \mathbf{X} \in \{0,1\}^{n_\mathrm{T} \times n_\mathrm{S}},\ \mathbf{X}\mathbf{1}_{n_\mathrm{S}} = \mathbf{1}_{n_\mathrm{T}},\ \mathbf{X}^T\mathbf{1}_{n_\mathrm{T}} \leq \mathbf{1}_{n_\mathrm{S}}. \end{aligned} \tag{7}$$

There are three constraints in (7) as follows.

1) $\mathbf{X} \in \{0,1\}^{n_\mathrm{T} \times n_\mathrm{S}}$ indicates a point-to-point matching pattern, where the matching between a template feature point and a scene feature point is either "Successful" ($X_{ij} = 1$) or "Failed" ($X_{ij} = 0$).
2) $\mathbf{X}\mathbf{1}_{n_\mathrm{S}} = \mathbf{1}_{n_\mathrm{T}}$ indicates that a template feature point exactly matches one scene feature point.
3) $\mathbf{X}^T\mathbf{1}_{n_\mathrm{T}} \leq \mathbf{1}_{n_\mathrm{S}}$ defines a one-to-one matching pattern, where a scene feature point is matched, at most, by one template feature point.

The problem in (7) has a nonlinear objective function with integer constraints. Such a formulation constructs an NP-hard problem and cannot be solved efficiently in polynomial time. To provide an approximately optimal solution, we develop a Linear Programming and Simulated Annealing (LPSA) algorithm. The LPSA algorithm starts by solving the following relaxed linear programming problem in a continuous space:

$$\begin{aligned} &\underset{\mathbf{X}}{\text{minimize}}\ \mathrm{tr}(\mathbf{C}\mathbf{X}^T) \\ &\text{subject to}\ \mathbf{X} \in [0,1]^{n_\mathrm{T} \times n_\mathrm{S}},\ \mathbf{X}\mathbf{1}_{n_\mathrm{S}} = \mathbf{1}_{n_\mathrm{T}},\ \mathbf{X}^T\mathbf{1}_{n_\mathrm{T}} \leq \mathbf{1}_{n_\mathrm{S}}. \end{aligned} \tag{8}$$

Solving the linear programming problem results in a continuous solution of $\mathbf{X}$. To map the continuous solution to a discrete integer solution space, for each row of $\mathbf{X}$, we simply set the entry with the maximum value to be 1; the others are set to be zero. Then, a simulated annealing procedure, based on (7), iteratively refines the initial solution. The simulated annealing procedure takes into consideration both feature and geometric matching costs. By iteratively adjusting the mismatched points based on geometric constraints, we finally obtain an optimal matching.

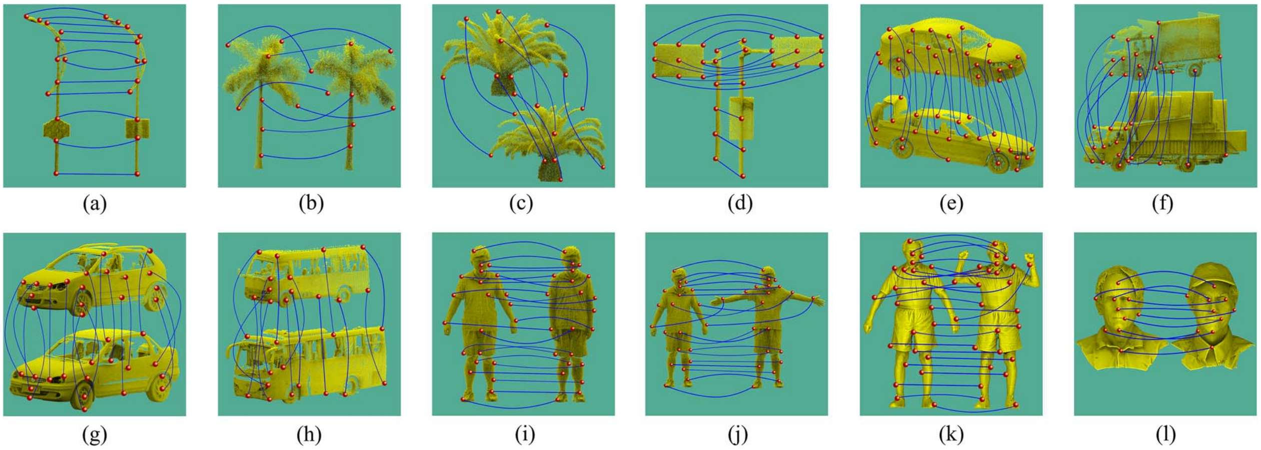

Fig. 1. (a)–(l) Correspondences computed with our framework.

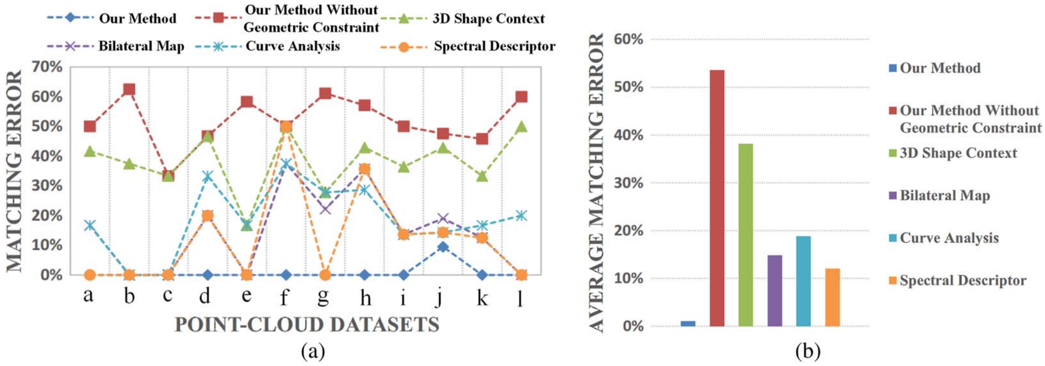

Fig. 2. (a) Matching errors and (b) average matching errors of different methods.

The LPSA algorithm works efficiently when both the number of template and scene feature points is small. When the number of feature points increases, the size of $\mathbf{X}$ increases dramatically. To reduce the computational complexity, we use a lower convex hull trick [17] to obtain the initial matching solution. In this way, only the scene feature points on the lower convex hull of the feature matching costs are considered as the matching candidates for each template feature point.

III. Results and Discussion

The 3-D point clouds used in this study were acquired by a RIEGL VMX-450 MLS system. This system integrates two full-view RIEGL VQ-450 laser scanners that generate a maximal effective measurement rate of 1.1 million measurements per second and a line scan speed of up to 400 scans per second. The accuracy and precision of the scanned point clouds are within 8 mm and 5 mm, respectively.

A. Three-Dimensional Correspondence

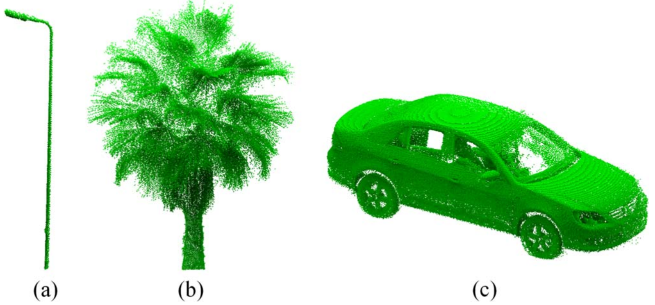

Fig. 3. Point cloud object prototypes of (a) light pole, (b) palm tree, and (c) car.

Here, we evaluate the performance of the proposed 3-D object matching framework in computing 3-D one-to-one correspondence in 3-D point clouds. First, we manually selected a group of salient feature points from the template and scene point clouds, respectively. Since we aimed to find one-to-one correspondences, we set the number of template and scene feature points to be identical, i.e., $n_{\mathrm{T}} = n_{\mathrm{S}}$. Next, we applied the proposed object matching framework to the selected data sets to compute one-to-one correspondences between template and scene feature points. We selected the neighbors of a feature point as the k-nearest neighboring feature points, where k was set at 5 in all of our experiments. We set the value of λ at 1.0 to assign equal weights to the feature and geometric matching costs. Fig. 1 shows the correspondences computed for 12 groups of 3-D point clouds, each of which contains a template object and a scene object.

We also compared the proposed 3-D object matching framework with several existing methods, including 3-D shape context [18], bilateral map [19], curve analysis [20], spectral descriptor [21], and our proposed framework without local geometric constraints. As shown in Fig. 2, the matching performance of different methods is evaluated by the matching errors represented by the percentage of mismatched template feature points. Comparatively, our method outperforms other

TABLE I
THREE-DIMENTIONAL OBJECT DETECTION AND QUANTITATIVE EVALUATION RESULTS

Dataset	Ground Truth	Detection Result			Quantitative Evaluation		
	Targets	Targets	Non-targets	Time	Completeness	Correctness	Quality
Light Pole	121	117	7	1924 s	0.967	0.944	0.914
Palm Tree	583	569	11	2412 s	0.976	0.981	0.958
Car	265	263	3	1013 s	0.992	0.989	0.981

methods and achieves a very low average matching error of 0.79%. Particularly, comparing the average matching errors obtained using our method with and without local geometric constraints (0.79% versus 51.87%), we conclude that performance is greatly improved when locally affine-invariant geometric constraints are considered.

B. Three-Dimensional Object Detection

Our 3-D object matching framework was embedded in a 3-D object detection method for detecting point cloud objects. First, the point clouds were preprocessed to remove ground points and segment off-ground points into clustered objects [2]. Next, by using the sampling method proposed in [22], n_{T} $(n_{\mathrm{T}} = 30)$ feature points were evenly sampled, respectively, from 1) each clustered object and 2) the point cloud object prototype representing an instance from a specific class of objects to be detected. Then, the object matching framework was carried out to match the feature points on the prototype to the feature points on each clustered object. The value of λ was set at 1.0, 3.0, and 2.0 for matching light poles, palm trees, and cars, respectively. Finally, the matching costs of all clustered objects were thresholded to determine the objects of interest. By receiver operating characteristic (ROC) curve analysis, the optimal thresholds selected for detecting light poles, palm trees, and cars were set at 1.4, 3.5, and 3.2, respectively.

In this letter, three data sets of MLS point clouds were selected for evaluating 3-D object detection performance. The first data set, containing 215 million points and covering a distance of about 1742 m in the road direction, was selected to evaluate the performance of light pole detection. The second data set, containing 320 million points and covering a length of about 1813 m along the road, was used to assess palm tree detection performance. The third data set, containing 185 million points and covering a road segment of about 881 m, was chosen for the evaluation of car detection performance. Fig. 3 shows the selected point cloud object prototypes of light poles, palm trees, and cars. The ground truth and detection results for these three data sets are detailed in Table I. "Targets" denotes the number of true positives; "Non-targets" denotes the number of false positives. The proposed method was implemented using C++ and executed on an HP Z820 workstation. The computing times for these three data sets are 1924, 2412, and 1013 s, respectively. Fig. 4 presents parts of the detection results for light poles, palm trees, and cars from the three data sets. To quantitatively evaluate the detection accuracy, three measures such as completeness (cpt), correctness (crt), and quality (qut) [23] were adopted. These three measures are defined as follows: $cpt = TP/(TP + FN), crt = TP/(TP + FP)$, and $qut = TP/(TP + FP + FN)$, where TP, FN, and FP denote the number of true positives, false negatives, and false positives, respectively. The evaluation results (see Table I) demonstrate that the proposed 3-D object matching framework is very promising.

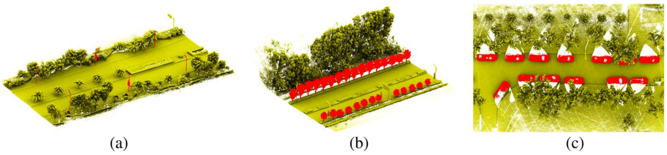

Fig. 4. Three-dimensional object detection results of (a) light poles, (b) palm trees, and (c) cars.

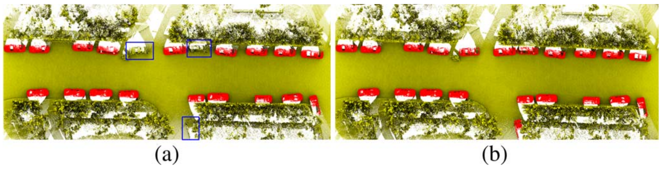

Fig. 5. Car detection results using (a) the method in [24] and (b) our method.

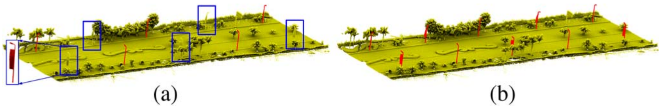

Fig. 6. Light pole detection results using (a) the method in [6] and (b) our method.

Comparative studies were also conducted to further compare the performance of the proposed method with an existing car detection method based on bottom-up and top-down descriptors [24] and a percentile-based light pole detection method [6]. The car and light pole detection results are shown in Figs. 5 and 6, respectively. As shown by the blue boxes in Figs. 5(a) and 6(a), some cars with extensive incompleteness and some light poles with advertising boards attached were not detected. However, such objects are correctly detected using our method. Thus, we conclude that our method is more effective and achieves better performance than the methods in [24] and [6].

C. Point Cloud Object Classification

As an extensive application, we integrated the object matching framework into a point cloud object classification method. The normalized cut classification algorithm [25] was used to classify point cloud objects into different categories. First, we organized the point cloud objects into a complete weighted graph, whose nodes are represented by the point cloud objects and whose edges are connected between each pair of nodes. Then, we evenly sampled n_{T} $(n_{\mathrm{T}} = 30)$ feature points from each point cloud object using the sampling method proposed in [22]. The weight w_{ij} on edge (i, j) was defined, using the matching cost between point cloud objects i and j, as follows:

$$w_{ij} = \exp\left(-\left(\mathrm{tr}(\mathbf{C}\mathbf{X}^T) + \lambda \left\|(\mathbf{I} - \mathbf{W})\mathbf{X}\mathbf{S}\right\|_1\right)\right). \quad (9)$$

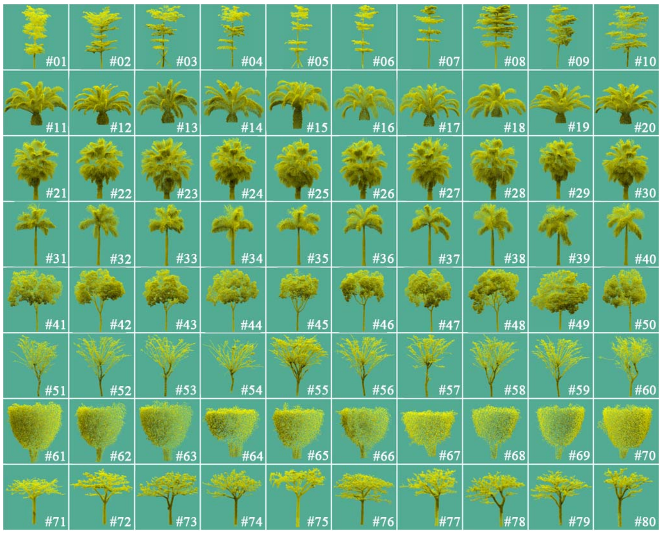

Fig. 7. Illustration of the point cloud objects for classification.

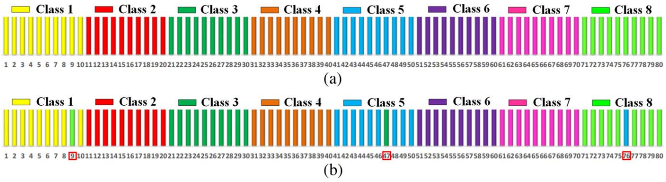

(a)

(b)

Fig. 8. (a) Ground truth and (b) point cloud object classification result.

Here, we set λ at 1.0 to assign equal weights to the feature and geometric matching costs. Finally, we applied the normalized cut classification algorithm to the weighted graph to classify the point cloud objects. In this letter, we selected 80 point cloud objects from 8 classes, each of which contains 10 instances (see Fig. 7). Fig. 8 details the ground truth and classification results. Our method achieves a classification error of 3.75%. Therefore, our method provides a promising and acceptable solution to point cloud object classification.

IV. Conclusion

This letter has presented a framework for 3-D object matching in 3-D MLS point clouds. A locally affine-invariant geometric constraint was proposed to improve the matching performance and handle the conditions of affine transformations, occlusions, incompleteness, and scales. Each feature point in 3-D MLS point clouds is locally represented by an affine combination of its neighbors. Such a representation results in an NP-hard problem of the overall objective function. As an approximately optimal solution, an LPSA algorithm was developed to provide a polynomial time solution. The proposed 3-D object matching framework was integrated into 3-D correspondence computation, 3-D object detection, and point cloud object classification. An average matching error of 0.79% was achieved in computing 3-D correspondence; a classification error of 3.75% was obtained on point cloud object classification. Through quantitative evaluations, our proposed method achieves a completeness, correctness, and quality of over 0.96, 0.94, and 0.91, respectively, on the detection of 3-D light poles, palm trees, and cars. Comparative studies also demonstrated that our method outperforms other methods in 3-D correspondence computation and 3-D object detection from MLS point clouds.

References

[1] K. Williams, M. J. Olsen, G. V. Roe, and C. Glennie, "Synthesis of transportation applications of mobile LiDAR," *Remote Sens.*, vol. 5, no. 9, pp. 4652–4692, Sep. 2013.

[2] Y. Yu, J. Li, J. Yu, H. Guan, and C. Wang, "Pairwise three-dimensional shape context for partial object matching and retrieval on mobile laser scanning data," *IEEE Geosci. Remote Sens. Lett.*, vol. 11, no. 5, pp. 1019–1023, May 2014.

[3] H. Wang *et al.*, "Object detection in terrestrial laser scanning point clouds based on Hough forest," *IEEE Geosci. Remote Sens. Lett.*, vol. 11, no. 10, pp. 1807–1811, Oct. 2014.

[4] Y. Yu, J. Li, H. Guan, and C. Wang, "Automated detection of road manhole and sewer well covers from mobile LiDAR point clouds," *IEEE Geosci. Remote Sens. Lett.*, vol. 11, no. 9, pp. 1549–1553, Sep. 2014.

[5] B. Yang, Z. Wei, Q. Li, and J. Li, "Automated extraction of street-scene objects from mobile LiDAR point clouds," *Int. J. Remote Sens.*, vol. 33, no. 18, pp. 5839–5861, Mar. 2012.

[6] S. Pu, M. Rutzinger, G. Vosselman, and S. O. Elberink, "Recognizing basic structures from mobile laser scanning data for road inventory studies," *ISPRS J. Photogramm. Remote Sens.*, vol. 66, no. 6, pp. S28–S39, Dec. 2011.

[7] B. Yang, Z. Wei, Q. Li, and J. Li, "Semiautomated building facade footprint extraction from mobile LiDAR point clouds," *IEEE Geosci. Remote Sens. Lett.*, vol. 10, no. 4, pp. 766–770, Jul. 2013.

[8] H. Fan, W. Yao, and L. Tang, "Identifying man-made objects along urban road corridors from mobile LiDAR data," *IEEE Geosci. Remote Sens. Lett.*, vol. 11, no. 5, pp. 950–954, May 2014.

[9] R. Wang, F. P. Ferrie, and J. Macfarlane, "A method for detecting windows from mobile LiDAR data," *Photogramm. Eng. Remote Sens.*, vol. 78, no. 11, pp. 1129–1140, Nov. 2012.

[10] B. Yang and L. Fang, "Automated extraction of 3D railway tracks from mobile laser scanning point clouds," *IEEE J. Sel. Topics Appl. Earth Observ. Remote Sens.*, to be published.

[11] B. Yang, L. Fang, and J. Li, "Semi-automated extraction and delineation of 3D roads of street scene from mobile laser scanning point clouds," *ISPRS J. Photogramm. Remote Sens.*, vol. 79, pp. 80–93, May 2013.

[12] A. Jochem, B. Höfle, and M. Rutzinger, "Extraction of vertical walls from mobile laser scanning data for solar potential assessment," *Remote Sens.*, vol. 3, no. 4, pp. 650–667, Mar. 2011.

[13] H. Guan *et al.*, "Using mobile laser scanning data for automated extraction of road markings," *ISPRS J. Photogramm. Remote Sens.*, vol. 87, pp. 93–107, Jan. 2014.

[14] R. B. Rusu, N. Blodow, Z. C. Marton, and M. Beetz, "Aligning point cloud views using persistent feature histograms," in *Proc. IEEE/RSJ Int. Conf. Intell. Robots Syst.*, Nice, France, 2008, pp. 3384–3391.

[15] E. Wahl, U. Hillenbrand, and G. Hirzinger, "Surflet-pair-relation histograms: A statistical 3D-shape representation for rapid classification," in *Proc. Int. Conf. 3-D Digit. Imag. Model.*, Banff, U.K., 2003, pp. 474–481.

[16] H. Li, X. Huang, and L. He, "Object matching using a locally affine invariant and linear programming techniques," *IEEE Trans. Pattern Anal. Mach. Intell.*, vol. 35, no. 2, pp. 411–424, Feb. 2013.

[17] H. Jiang, M. S. Drew, and Z. N. Li, "Matching by linear programming and successive convexification," *IEEE Trans. Pattern Anal. Mach. Intell.*, vol. 29, no. 6, pp. 959–975, Jun. 2007.

[18] M. Körtgen, G. J. Park, M. Novotni, and R. Klein, "3D shape matching with 3D shape contexts," in *Proc. Central Eur. Semin. Comput. Graph.*, Wien, Austria, 2003, vol. 3, pp. 5–17.

[19] O. van Kaick, H. Zhang, and G. Hamarneh, "Bilateral maps for partial matching," *Comput. Graph. Forum*, vol. 32, no. 6, pp. 189–200, Sep. 2013.

[20] H. Tabia, M. Daoudi, J. P. Vandeborre, and O. Colot, "A new 3D-matching method of nonrigid and partially similar models using curve analysis," *IEEE Trans. Pattern Anal. Mach. Intell.*, vol. 33, no. 4, pp. 852–858, Apr. 2011.

[21] R. Litman and A. M. Bronstein, "Learning spectral descriptors for deformable shape correspondence," *IEEE Trans. Pattern Anal. Mach. Intell.*, vol. 36, no. 1, pp. 171–180, Jan. 2014.

[22] D. P. Mitchell, "Spectrally optimal sampling for distribution ray tracing," *ACM SIGGRAPH Comput. Graph.*, vol. 25, no. 4, pp. 157–164, Jul. 1991.

[23] M. Rutzinger, F. Rottensteiner, and N. Pfeifer, "A comparison of evaluation techniques for building extraction from airborne laser scanning," *IEEE J. Sel. Topics Appl. Earth Observ. Remote Sens.*, vol. 2, no. 1, pp. 11–20, Mar. 2009.

[24] A. Patterson, IV, P. Mordohai, and K. Daniilidis, "Object detection from large-scale 3D datasets using bottom-up and top-down descriptors," in *Eur. Conf. Comput. Vis.*, Marseille, France, 2008, pp. 553–566.

[25] J. Shi and J. Malik, "Normalized cuts and image segmentation," *IEEE Trans. Pattern Anal. Mach. Intell.*, vol. 22, no. 8, pp. 888–905, Aug. 2000.